

Vortex dynamics in a NbN film studied by terahertz spectroscopy

Y. Ikebe,¹ R. Shimano,^{1,2,*} M. Ikeda,³ T. Fukumura,^{2,3} and M. Kawasaki^{3,4,5}

¹*Department of Physics, The University of Tokyo, Tokyo 113-0033, Japan*

²*PRESTO, Japan Science and Technology Agency, Tokyo 102-0075, Japan*

³*Institute for Materials Research, Tohoku University, Sendai 980-8577, Japan*

⁴*WPI Advanced Institute for Materials Research, Tohoku University, Sendai 980-8577, Japan*

⁵*CREST, Japan Science and Technology Agency, Tokyo 102-0075, Japan*

(Received 10 March 2009; revised manuscript received 14 April 2009; published 22 May 2009)

We have investigated the effect of vortex dynamics on high-frequency conductivity of a superconducting NbN film by using terahertz time-domain spectroscopy. The complex conductivity of the mixed state up to 7 T is determined without using Kramers-Kronig analysis. The experimentally obtained conductivity spectra are analyzed by considering the contribution from quasiparticles in vortices and also from the vortex dynamics. To include the local-field effect in the high-frequency electromagnetic responses of mixed-state superconductors, we combined the Maxwell-Garnett theory with a self-consistent two-fluid model and obtained the expression for the effective conductivity. The volume fraction of the vortices shows the linear dependence on the applied magnetic field, as expected for *s*-wave superconductors, by taking into account the flux-flow resistivity.

DOI: [10.1103/PhysRevB.79.174525](https://doi.org/10.1103/PhysRevB.79.174525)

PACS number(s): 74.25.Gz, 74.78.Db, 74.25.Nf, 74.25.Op

I. INTRODUCTION

The vortex dynamics has been intensively investigated to understand transport properties of superconductors (SCs) under the magnetic field both from fundamental¹⁻⁵ and applicational⁶⁻⁹ points of view. Effects of vortex dynamics on the conductivity can be characterized by a few fundamental parameters such as viscosity and pinning force, which govern the dynamics of SCs in the mixed state. Since the typical depinning frequency locates at rf region for conventional SCs (Ref. 10) and at 10–100 GHz for high- T_c SCs,¹¹ the high-frequency electromagnetic response of vortices has been intensively studied.¹⁰⁻¹⁴

With the progress of terahertz time-domain spectroscopy (THz-TDS),¹⁵ the energy range has been further extended, making it possible to obtain directly the complex conductivity spectra without using Kramers-Kronig analysis. Especially, since the relevant frequency is much higher than the depinning frequency even for high- T_c SCs, the technique makes it possible to obtain the resistivity in the flux-flow region by optical means.¹⁶

Such high-frequency optical characterization can also be applied to conventional SCs to reveal not only the gap structures¹⁷⁻¹⁹ but also the vortex dynamics. For this purpose, we employed THz-TDS under the high magnetic field,²⁰ and applied the technique to a NbN film, which exhibits a relatively high T_c among the conventional SCs with a strong pinning.

To describe the ac-electromagnetic response of mixed-state SCs, Coffey and Clem²¹ introduced an effective model which took into account the dissipation due to vortex dynamics in the frame work of two-fluid model and successfully explained the results in microwave range. However, since the two-fluid model does not take into account the local-field effect on the vortices, the validity of the model should be examined in particular for the high-frequency electromagnetic responses of mixed-state SCs. In this paper, we consider the local-field effect based on Maxwell-Garnett

theory²² and modify the Coffey-Clem self-consistent theory. As a result, we reveal how vortices contribute to the ac conductivity in the THz frequency range.

II. THEORETICAL MODEL

Under the magnetic field, magnetic fluxes penetrate into SCs as vortices, and largely affect the conductivity through the contribution from quasiparticles in vortices and also from the contribution due to the vortex dynamics. In dc response, the contribution from the quasiparticles inside the vortices is negligible because of the infinite conductivity of the surrounding superconducting state. In contrast, in the high-frequency range, the contribution of quasiparticles in vortices as well as vortex dynamics should be taken into account. According to the Coffey and Clem's model,²¹ these effects are described by introducing the relation of vortex displacement and the current density self-consistently as follows. At zero temperature, the current density due to quasiparticles in vortices, \mathbf{I}_n , and the superconducting current density outside the vortices, \mathbf{I}_s , are written as

$$\mathbf{I}_n = f\sigma_n\mathbf{E}, \quad (1)$$

$$\nabla \times \mathbf{I}_s = -\frac{1}{\mu_0\lambda^2}(\mathbf{B} - \phi_0 n\hat{\mathbf{z}}), \quad (2)$$

where σ_n is the normal-state conductivity inside the vortices, f is the volume fraction of vortices which is described by using the upper critical field H_{c2} as $f=B/H_{c2}$ for *s*-wave SCs, μ_0 is the permeability of vacuum, $\phi_0=h/(2e)$ is the flux quantum, $\hat{\mathbf{z}}$ is the unit vector along the magnetic flux, $n(\mathbf{x}, t)$ is the vortex density, and λ is the penetration depth which is expressed by the conductivity of superconducting state σ_s , as $\lambda^{-2}=-i\omega\mu_0(1-f)\sigma_s$. Here the magnetic field \mathbf{B} is represented as a summation of ac-electromagnetic wave \mathbf{B}_{ac} and magnetic fluxes of vortices \mathbf{B}_0 . Although $\phi_0 n\hat{\mathbf{z}}$ corresponds to \mathbf{B}_0 when the vortex does not move, the dissipation caused

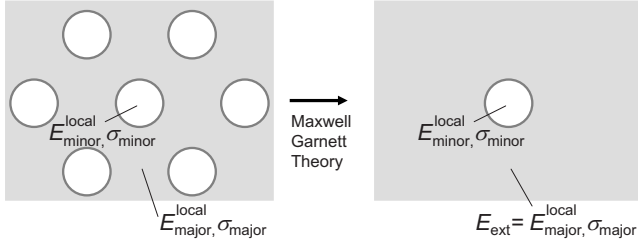


FIG. 1. Concept of Maxwell-Garnett theory. The local field of the spatially minor component is calculated by assuming external field which is equivalent of the local field of the major component.

by vortex dynamics generates the additional magnetic field which depends on the current density. Then, by considering the total current density $\mathbf{I}=\mathbf{I}_n+\mathbf{I}_s$, the generalized diffusion London equation for \mathbf{B} can be obtained as

$$\nabla^2\mathbf{B}=f\mu_0\sigma_n\dot{\mathbf{B}}+\frac{1}{\lambda^2}(\mathbf{B}-\phi_0n\hat{\mathbf{z}}). \quad (3)$$

By solving the equation self-consistently, Coffey and Clem expressed the frequency-dependent complex penetration depth of the mixed state. In terms of the conductivity, their result [Eq. (4) in Ref. 21] is equivalently represented as

$$\sigma_{\text{all}}=\frac{(1-f)\sigma_s+f\sigma_n}{1+(1-f)\sigma_s/\sigma_{\text{vd}}}, \quad (4)$$

where σ_{vd} is the conductivity induced by the vortex dynamics.

In order to include the contribution of the local-field effect, we replace the inner and outer vortex conductivities σ_n and σ_s with the effective values σ_n^{eff} and σ_s^{eff} . σ_n^{eff} and σ_s^{eff} are defined by using the macroscopic electric field E and their local current density, $I_{n(s)}^{\text{local}}$, without the contribution of vortex dynamics as, $\sigma_{n(s)}^{\text{eff}}=I_{n(s)}^{\text{local}}/E$.

By using Maxwell-Garnett theory,²² we describe σ_n^{eff} and σ_s^{eff} as follows. In Maxwell-Garnett theory, the local field of the minor component is described by assuming that the minor component is surrounded by a uniform medium composed of the major component and feels the external field that coincides with the local field for the major component (see Fig. 1). Then the macroscopic electric field and current density are described as spatial average of the local field of a minor and a major component. We applied the theory to SCs by considering the inner and outer vortex regions as a minor and a major component, respectively. The shape of vortex region is assumed as a cylinder which has radius of the coherence length ξ . In our experimental condition, where the cylindrical axis $\hat{\mathbf{z}}$ is parallel to THz wave vector, the electric field at each region is expressed by using Maxwell-Garnett theory as

$$E_n^{\text{local}}=I_n^{\text{local}}/\sigma_n=\frac{2\sigma_s}{\sigma_s+\sigma_n}E_s^{\text{local}}, \quad (5)$$

$$E_s^{\text{local}}=I_s^{\text{local}}/\sigma_s, \quad (6)$$

where $E_{n(s)}^{\text{local}}$ is the local electric field in normal (superconducting) state. Then the effective conductivity of the inner

and the outer vortex regions can be represented from the macroscopic electric field $E=fE_n^{\text{local}}+(1-f)E_s^{\text{local}}$ as

$$\begin{aligned} f\sigma_n^{\text{eff}} &= f\frac{I_n^{\text{local}}}{E} = \frac{f\sigma_n E_n^{\text{local}}}{fE_n^{\text{local}}+(1-f)E_s^{\text{local}}} \\ &= \sigma_n \left(1 + \frac{1-f}{f} \frac{\sigma_n + \sigma_s}{2\sigma_s}\right)^{-1}, \end{aligned} \quad (7)$$

$$\begin{aligned} (1-f)\sigma_s^{\text{eff}} &= (1-f)\frac{I_s^{\text{local}}}{E} = \frac{(1-f)\sigma_s E_s^{\text{local}}}{fE_n^{\text{local}}+(1-f)E_s^{\text{local}}} \\ &= \sigma_s \left(1 + \frac{f}{1-f} \frac{2\sigma_s}{\sigma_n + \sigma_s}\right)^{-1}. \end{aligned} \quad (8)$$

Moreover, the macroscopic effective conductivity $\sigma_{\text{eff}}=f\sigma_n^{\text{eff}}+(1-f)\sigma_s^{\text{eff}}$ is written as

$$\sigma_{\text{eff}}=\frac{2f\sigma_s(\sigma_n-\sigma_s)}{(1-f)(\sigma_n-\sigma_s)+2\sigma_s}+\sigma_s. \quad (9)$$

On the other hand, the contribution of vortex dynamics is considered from the equation of motion

$$\eta\mathbf{v}_L+\kappa\mathbf{x}_L=\phi_0\mathbf{I}\times\hat{\mathbf{z}}, \quad (10)$$

where \mathbf{x}_L and \mathbf{v}_L is the position and the velocity of vortex, \mathbf{I} is the current density, η is the viscosity, and κ is the pinning force. For high-frequency responses where $\omega\gg\kappa/\eta$ is satisfied, the second term of the left-hand side in Eq. (10) can be ignored, and by using the Josephson relation,²³ $\mathbf{E}=\mathbf{B}\times\mathbf{v}_L$, the flux-flow conductivity is represented as $\sigma_{\text{vd}}=\eta/(B\phi_0)$. In addition, using the expression of viscosity $\eta=\phi_0B\sigma_n/f$ by Bardeen and Stephen,²⁴ the conductivity is written in a simple form as

$$\sigma_{\text{vd}}=\frac{\sigma_n}{f} \quad (11)$$

which corresponds to the normal-state conductivity σ_n at the upper critical field $f=1$. Finally, from Eq. (4), we can express the whole conductivity which includes the contribution from the vortex dynamics as

$$\sigma_{\text{all}}=\frac{\sigma_{\text{eff}}}{1+(1-f)\sigma_s^{\text{eff}}/\sigma_{\text{vd}}}. \quad (12)$$

It should be noted here that this conductivity approaches to the original model by Coffey-Clem, Eq. (4), in low-frequency region where $|\sigma_s|$ has much larger value than $|\sigma_n|$. Thus the local-field effect gives the negligible contribution in the microwave region where $|\sigma_s|\gg|\sigma_n|$ is satisfied while it is not necessarily negligible in THz frequency range.

III. EXPERIMENTS

In this section we describe our experimental setup and the results. The experimental setup is schematically shown in Fig. 2. As a light source, we used a mode-locked Titanium-Sapphire laser, with pulse width of 110 fs, center wavelength of 800 nm, and repetition frequency of 76 MHz. THz wave is generated by focusing the laser pulse onto a p -type (111)

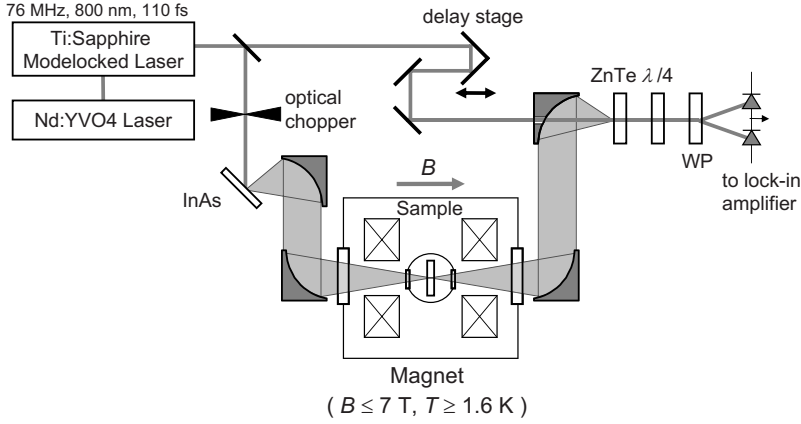


FIG. 2. Schematic experimental setup. $\lambda/4$: quarter-wave plate. WP: wollaston prism.

InAs surface and detected by electro-optical sampling using a (110) ZnTe crystal.

Samples are inserted in a split-type superconducting magnet which can produce the magnetic field up to 7 T in Faraday configuration. The experimental setup with the magnet enables the transmission-type spectroscopy in the frequency range from 1.5 to 8.4 meV (0.4 to 2.0 THz). Further details of the experimental setup are described in Ref. 20.

As a sample, we used a 240-Å-thick NbN film which is epitaxially grown on a 500- μm -thick MgO (100) substrate by using the pulsed laser deposition technique. A MgO crystal of the same thickness of 500 μm is also used as a reference. The transition temperature of the film is $T_c=15.1$ K which corresponds to the superconducting gap energy of $2\Delta=4.59$ meV(=1.11 THz) in BCS theory. Figure 3(a) shows the temperature dependence of the dc resistivity under the magnetic field applied perpendicular to the film. Temperature dependence of the upper critical field $H_{c2}(a \equiv T/T_c)$ is plotted in Fig. 3(b) from which the zero-temperature value is estimated as $H_{c2}(0)=12.9$ T by using the relation,²⁵

$$H_{c2}(a) = H_{c2}(0) \frac{1 - a^2}{1 + a^2}. \quad (13)$$

The coherence length ξ is then estimated as $\xi=50.5$ Å from the relation, $H_{c2} = \phi_0 / (2\pi\xi^2)$.

In the analysis of the THz transmittance of a thin metal film on a thick substrate, multiple reflections inside the substrate can be avoided in time domain since THz-TDS records the time-domain wave form of the electric field. However,

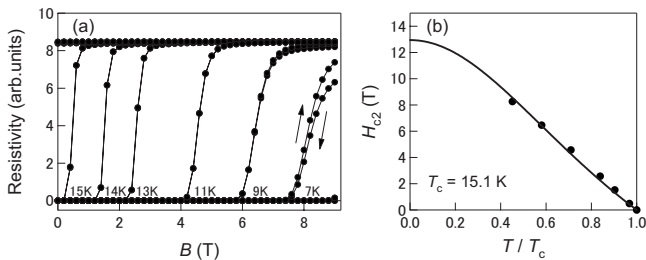


FIG. 3. (a) Magnetic-field dependence of the dc resistivity. (b) Temperature dependence of the upper critical field H_{c2} . Solid line represents fitting by Eq. (13).

the effect of multiple reflections inside the thin film should be taken into account (see Appendix). In the thin-film limit, the complex transmittance $t(\omega)$ can be written by using the complex conductivity of the film σ , the film thickness d , and the refractivity of the substrate n_{sub} as

$$t(\omega) = \frac{1}{Z_0 d \sigma(\omega) + n_{\text{sub}} + 1} \frac{4n_{\text{sub}} e^{i\Phi(\omega)}}{n_{\text{sub}} + 1}, \quad (14)$$

where Z_0 is the vacuum impedance and $\Phi(\omega) = (n_{\text{sub}} d_{\text{sub}} - d - d_{\text{sub}})\omega/c$ (d_{sub} : the substrate thickness) is the phase component which is independent of σ . In THz-TDS, the wave form of the transmitted electric field is directly measured which contains both the amplitude and the phase information. Accordingly, the complex transmittance $t(\omega)$ is obtained from the Fourier transformation of the wave form and then the complex conductivity of the film is retrieved by numerically solving Eq. (14).

Figure 4 shows the obtained complex conductivity spectra of the NbN film at $T=3$ K and $T=20$ K without magnetic field. Superconducting gap structure is clearly observed in the real part of the conductivity at 3 K. The dominant contribution to the error is caused by the systematic error of the time scan in THz-TDS. The solid line in Fig. 4 is a theoretical fitting by Mattis-Bardeen model with arbitrary electron mean-free path,²⁶ where the least-squares method is applied to the real part of σ in the frequency range from 5.9 to 10.2

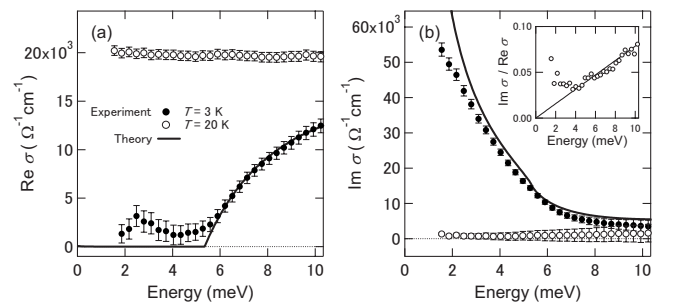


FIG. 4. (a) The real part and (b) the imaginary part of the conductivity spectra in the superconducting state, $T=3$ K (closed circles), and in the normal state, $T=20$ K (open circles). Solid line represents the theoretical fitting by Mattis-Bardeen model. The inset shows the ratio of real and imaginary parts in the normal-state conductivity at $T=20$ K (open circles) and the fitting curve (line).

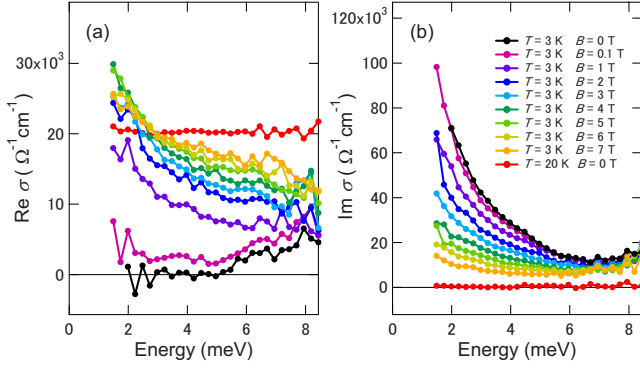


FIG. 5. (Color online) (a) The real part and (b) the imaginary part of the complex conductivity under the indicated magnetic field at 3 K. The spectrum in the normal state at 20 K without the magnetic field is also plotted.

meV. From the fitting, the relaxation time τ_s of the superconducting state is estimated as 10 ± 10 fs and the gap energy at zero temperature as $2\Delta = 5.3_{-0.1}^{+0.2}$ meV. The resulting value of $2\Delta/(k_B T_c) = 4.1 \pm 0.1$ is larger than the value expected from BCS theory of $2\Delta/(k_B T_c) = 3.52$, indicating the strong electron-phonon coupling.²⁷ The inset of Fig. 4 plots the ratio of the real and the imaginary parts of the normal-state conductivity, which is expressed as $\text{Im}[\sigma]/\text{Re}[\sigma] = \omega\tau_n$ within the Drude model by using the relaxation time of the normal state τ_n . From the slope, τ_n is estimated as 5_{-5}^{+8} fs.

Figure 5 plots the magnetic-field dependence of the complex conductivity of the NbN film at 3 K. By applying the magnetic field perpendicular to the film, we observed the recovery of the missing spectral weight approaching to the value of normal state at $T=20$ K. This recovery of the spectral weight can be attributed to the increase in vortices. The observed magnetic-field dependence is fitted by Eq. (12) by using the volume fraction f of vortices as a fitting parameter. We substitute the experimentally observed conductivity $\sigma(B=0 \text{ T}, T=3 \text{ K})$ and $\sigma(B=0 \text{ T}, T=20 \text{ K})$ for σ_s and σ_n in Eq. (12), respectively. It should be noted here that the quasiparticle bound states can exist in a system with short coherence length, as observed in the clean-limit conventional SC, NbSe₂ (Ref. 28), or in high- T_c SCs.^{13,29} In the present case of NbN, however, the system can be recognized as dirty limit. In such a case, the bound states in the vortex core are considered to disappear and the conductivity inside the vortex can be regarded as that of normal state.³⁰ The theoretical fitting obtained by Eq. (12) is shown in Fig. 6 as solid lines. To avoid the effect due to quasiparticle excitation above the gap energy, we restrict the fitting range from 2.2 to 4.5 meV. For comparison, dashed lines in Fig. 6 represent the conductivity fitted without the contribution of vortex dynamics. Especially in the real part of the conductivity, the fitting with vortex dynamics gives a better fitting.

Since the volume fraction f is obtained from the above analysis, we plot the magnetic-field dependence of f in Fig. 7. Both the results obtained from the analysis with and without the contribution of vortex dynamics are plotted. Linear dependence of the volume fraction on the magnetic field is clearly observed by considering the vortex dynamics, which is expected for s -wave SCs. On the other hand, the sublinear

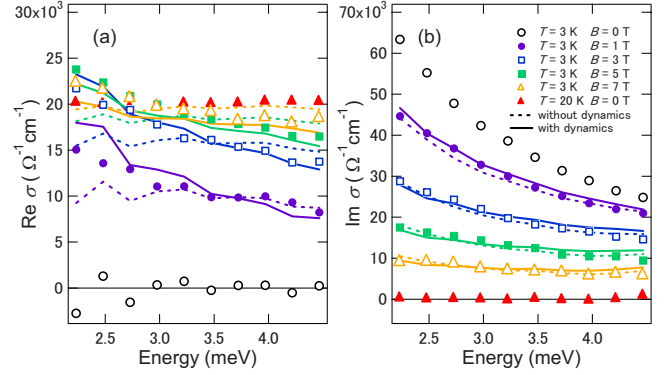


FIG. 6. (Color online) Theoretical fittings of the complex conductivity by using the modified Coffey-Clem theory which takes into account the local-field effect of the vortex. (a): real part and (b): imaginary part. Lines represent the theoretical fitting with (solid line) and without (dashed line) the vortex dynamics, respectively.

dependence is obtained when the effect of vortex dynamics is not taken into account. This result indicates the significant contribution of vortex dynamics on the THz responses of the mixed-state SCs. By extrapolating $f(B)$ for the results with vortex dynamics, the upper critical field H_{c2} is estimated as $H_{c2} = 12.7$ T from the value at $f=1$, showing good correspondence with the value estimated from the dc measurement; $H_{c2}(3 \text{ K}/15.1 \text{ K}) = 11.9$ T.

IV. COMPARISON WITH THE ORIGINAL COFFEY-CLEM SELF-CONSISTENT THEORY

In this section, we compare our model [Eq. (12)] with the original Coffey-Clem theory [Eq. (4)] to examine the influence of the local-field effect. For this purpose we assume that the volume fraction is *a priori* expressed as $f(B) = B/H_{c2}$ and determine the flux-flow conductivity σ_{vd} from the results shown in Fig. 5 by using these two models. Different from the previous section, the flux-flow conductivity σ_{vd} can be estimated directly from the observed σ_{all} without any fitting, as shown in Fig. 8 in the form of the flux-flow resistivity

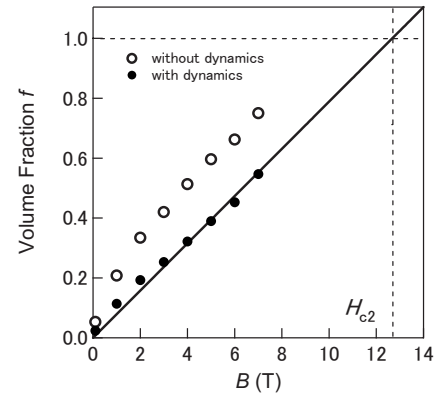


FIG. 7. Magnetic-field dependence of the volume fraction f estimated from the analysis with (closed circles) and without (open circles) the vortex dynamics, respectively. Solid line represents a linear fitting.

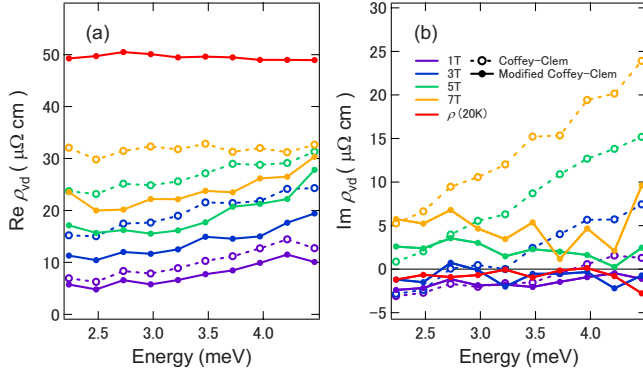


FIG. 8. (Color online) (a) The real part and (b) the imaginary part of the flux-flow resistivity estimated from Fig. 5 by using the modified Coffey-Clem theory (solid line) and the original Coffey-Clem theory (dashed line) under the indicated magnetic field. The normal-state resistivity without magnetic field is also plotted as a reference.

$\rho_{vd} = 1 / \sigma_{vd}$. In Fig. 8, $\text{Re } \rho_{vd}$ monotonically increases with B as expected from Eq. (11) for both models. On the other hand, $\text{Im } \rho_{vd}$ shows completely different behavior between these models; our model gives nearly zero value for the whole frequency range which is equivalent to Eq. (11), whereas the original Coffey-Clem model gives linearly increasing values with frequency. As previously mentioned, this irregular behavior can be attributed due to the two-fluid model which neglects the local-field effect. Since in the THz frequency range, the condition $|\sigma_s| \gg |\sigma_n|$ does not hold, the two-fluid model causes such an artifact.

We also compared the magnetic-field dependence of $\text{Re } \rho_{vd}$ estimated from both models. In Fig. 9, the value of $\text{Re } \rho_{vd}$ is averaged between 2.2 and 4.5 meV to smooth the scattered data. Although the difference between two models is not significant, the present model seems to give a better correspondence with the theoretical value [Eq. (11)].

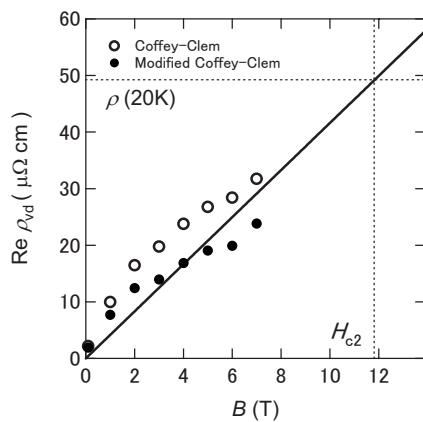


FIG. 9. Magnetic-field dependence of the flux-flow resistivity by using the modified Coffey-Clem theory (closed circles) and the original Coffey-Clem theory (open circles). Solid line represents the theoretical value calculated by using the upper critical field $H_{c2}(3 \text{ K}/15.1 \text{ K}) = 11.9 \text{ T}$.

V. SUMMARY

In this paper, we have investigated the electromagnetic response of a superconducting NbN film under the magnetic field by THz-TDS. In order to examine the local-field effect as well as the role of vortex dynamics, we have constructed an effective theory by modifying the Coffey-Clem self-consistent theory. The complex conductivity spectra under the magnetic field up to 7 T are obtained in the frequency range between 1.5 and 8.4 meV (0.4 –2.0 THz). The magnetic-field dependence of the volume fraction of vortices shows a linear dependence on the applied magnetic field B as expected for the s -wave superconductor, when the contribution from the flux flow resistivity is taken into account. The effect of the local field on vortices is also examined by comparing the analysis based on the original Coffey-Clem theory, showing the importance of the local-field effect in the high-frequency responses of SCs where $|\sigma_s|$ becomes comparable with $|\sigma_n|$. In addition, by estimating the volume fraction of vortices, the upper critical field is determined by optical means.

ACKNOWLEDGMENTS

We thank Y. Onose for the dc-resistivity measurement under the magnetic field. This work is in part supported by Global COE Program “the Physical Sciences Frontier,” MEXT, Japan.

APPENDIX: DETERMINATION OF THE CONDUCTIVITY BY THz-TDS

Here we introduce our method of analysis to obtain the complex conductivity of sample by using THz-TDS. In THz-TDS, the temporal wave form of the THz electric field is recorded which contains the information of the amplitude and the phase. Since the transmitted amplitude and the phase of the electric field are related to the complex conductivity of the medium, we can obtain the complex conductivity of sample without using Kramers-Kronig analysis.

First, we consider a thick sample without taking into account the effect of the multiple reflections inside the sample. Experimentally, such a condition is realized by avoiding the signal due to the multiple reflections in time domain. In such a case, the transmitted electric field after the sample, E_{out} , is expressed in frequency domain as¹⁵

$$E_{\text{out}}(\omega, n, d) = E_{\text{in}}(\omega) \frac{4n}{(n+1)^2} e^{ind\omega/c}, \quad (\text{A1})$$

where $E_{\text{in}}(\omega)$ is the incident electric field, and n and d are the complex refractivity and the thickness of the sample, respectively. In THz-TDS, one measures the wave forms of the electric field with and without the sample, and then obtain their Fourier transforms $E_{\text{sample}}(\omega)$ and $E_{\text{blank}}(\omega)$. Then the complex transmittance is obtained from Eq. (A1) as

$$t(\omega) = \frac{E_{\text{sample}}(\omega)}{E_{\text{blank}}(\omega)} = \frac{E_{\text{out}}(\omega, n, d)}{E_{\text{out}}(\omega, 1, d)} = \frac{4n}{(n+1)^2} e^{i(n-1)d\omega/c}. \quad (\text{A2})$$

By solving Eq. (A2) inversely in terms of n , one can determine n without using the Kramers-Kronig analysis. From the obtained complex refractivity, the complex dielectric constant ϵ and the complex conductivity σ are calculated by using the relations,

$$\epsilon = n^2, \quad (\text{A3})$$

$$\sigma = -i\epsilon_0(\epsilon - \epsilon_b)\omega, \quad (\text{A4})$$

where ϵ_0 and ϵ_b is the dielectric constant of vacuum and background. ϵ_b can be ignored in the case of $|\epsilon| \gg \epsilon_b$, which is generally satisfied for metals and SCs.

Next, we consider the case of a thin metal film on a thick substrate. As mentioned previously, the multiple reflections inside the thick substrate can be avoided in time domain and we take into account the multiple reflections only inside the thin film. The transmitted electric field $E_{\text{out}}^{\text{mr}}(\omega)$ is then represented as summation of $2m$ -times reflected waves as

$$E_{\text{out}}^{\text{mr}}(\omega) = E_{\text{in}}(\omega) \frac{8n_1n_2}{(n_1+1)(n_1+n_2)(n_2+1)} \times e^{i(n_1d_1+n_2d_2)\omega/c} \sum_{m=0}^{\infty} \left\{ \frac{n_1-1}{n_1+1} \frac{n_1-n_2}{n_1+n_2} e^{2in_1d_1\omega/c} \right\}^m, \quad (\text{A5})$$

where $n_{1(2)}$ and $d_{1(2)}$ is the complex refractivity and the

thickness of the film (substrate), respectively. By measuring the electric field without the sample, $E_{\text{blank}}(\omega) = E_{\text{out}}(\omega, 1, d_1 + d_2)$, then the complex transmittance can be written as

$$t(\omega) = \frac{E_{\text{out}}^{\text{mr}}(\omega)}{E_{\text{out}}(\omega, 1, d_1 + d_2)} = \frac{8n_1n_2}{(n_1+1)(n_1+n_2)(n_2+1)} \frac{e^{i[(n_1-1)d_1+(n_2-1)d_2]\omega/c}}{1 - \frac{n_1-1}{n_1+1} \frac{n_1-n_2}{n_1+n_2} e^{2in_1d_1\omega/c}}. \quad (\text{A6})$$

When the refractivity of the film $|n_1|$ has very large value and the thickness d_1 is very thin so as to satisfy $|n_1\omega d_1/c| \ll 1$, $|n_1| \gg |n_2|$, and $|\epsilon_1| \gg \epsilon_{1b}$ (ϵ_1 : the dielectric constant of the film, ϵ_{1b} : the background dielectric constant), this expression can be simplified as

$$t(\omega) = \frac{1}{Z_0 d_1 \sigma_1(\omega) + n_2 + 1} \frac{4n_2 e^{i\Phi(\omega)}}{n_2 + 1}, \quad (\text{A7})$$

where $Z_0 = 377 \Omega$ is the vacuum impedance, σ_1 is the conductivity of the film, and $\Phi(\omega) = (n_2 d_2 - d_1 - d_2)\omega/c$ is the phase component which is independent of σ_1 .

*Author to whom correspondence should be addressed; shimano@phys.s.u-tokyo.ac.jp

¹M. P. A. Fisher, Phys. Rev. Lett. **62**, 1415 (1989).

²D. S. Fisher, M. P. A. Fisher, and D. A. Huse, Phys. Rev. B **43**, 130 (1991).

³R. H. Koch, V. Foglietti, W. J. Gallagher, G. Koren, A. Gupta, and M. P. A. Fisher, Phys. Rev. Lett. **63**, 1511 (1989).

⁴P. L. Gammel, L. F. Schneemeyer, and D. J. Bishop, Phys. Rev. Lett. **66**, 953 (1991).

⁵H. K. Olsson, R. H. Koch, W. Eidelloth, and R. P. Robertazzi, Phys. Rev. Lett. **66**, 2661 (1991).

⁶T. Koyama and M. Tachiki, Solid State Commun. **96**, 367 (1995).

⁷M. Tachiki, M. Iizuka, K. Minami, S. Tejima, and H. Nakamura, Phys. Rev. B **71**, 134515 (2005).

⁸J. E. Villegas, S. Savel'ev, F. Nori, E. M. Gonzalez, J. V. Anguita, R. García, and J. L. Vicent, Science **302**, 1188 (2003).

⁹C. C. de Souza Silva, J. Van de Vondel, M. Morelle, and V. V. Moshchalkov, Nature (London) **440**, 651 (2006).

¹⁰J. I. Gittleman and B. Rosenblum, Phys. Rev. Lett. **16**, 734 (1966).

¹¹M. Golosovsky, M. Tsindlekht, H. Chayet, and D. Davidov, Phys. Rev. B **50**, 470 (1994).

¹²B. Rosenblum and M. Cardona, Phys. Rev. Lett. **12**, 657 (1964).

¹³A. Maeda, H. Kitano, K. Kinoshita, T. Nishizaki, K. Shibata, and N. Kobayashi, J. Phys. Soc. Jpn. **76**, 094708 (2007).

¹⁴For a review, see, e.g., M. Golosovsky, M. Tsindlekht, and D. Davidov, Supercond. Sci. Technol. **9**, 1 (1996).

¹⁵M. C. Nuss and J. Orenstein, in *Millimeter and Submillimeter Wave Spectroscopy of Solids*, edited by G. Grüner (Springer-Verlag, Berlin, 1998), Chap. 2, pp. 7–50.

¹⁶J. Orenstein, R. P. Mallozzi, and B. Parks, in *The Superconducting State in Magnetic Fields: Special Topics and New Trends*, edited by C. A. R. Sá de Melo (World Scientific, Singapore, 1998), Chap. 9, pp. 150–174.

¹⁷M. C. Nuss, K. W. Goossen, J. P. Gordon, P. M. Mankiewich, M. L. O'malley, and M. Bhushan, J. Appl. Phys. **70**, 2238 (1991).

¹⁸R. A. Kaindl, M. A. Carnahan, J. Orenstein, D. S. Chemla, H. M. Christen, H.-Y. Zhai, M. Paranthaman, and D. H. Lowndes, Phys. Rev. Lett. **88**, 027003 (2001).

¹⁹T. Mori, E. J. Nicol, S. Shiizuka, K. Kuniyasu, T. Nojima, N. Toyota, and J. P. Carbotte, Phys. Rev. B **77**, 174515 (2008).

²⁰Y. Ikebe and R. Shimano, Appl. Phys. Lett. **92**, 012111 (2008).

²¹M. W. Coffey and J. R. Clem, Phys. Rev. Lett. **67**, 386 (1991).

²²G. L. Carr, S. Perkowitz, and D. B. Tanner, in *Infrared and Millimeter Waves*, edited by K. J. Button (Academic, Orlando, 1985), Vol. 13, Chap. 6, pp. 171–263.

²³B. D. Josephson, Phys. Lett. **16**, 242 (1965).

- ²⁴J. Bardeen and M. J. Stephen, Phys. Rev. **140**, A1197 (1965).
- ²⁵M. Tinkham, *Introduction to Superconductivity*, 2nd ed. (McGraw-Hill, New York, 1996), Chap. 4, pp. 110–147.
- ²⁶W. Zimmermann, E. H. Brandt, M. Bauer, E. Seider, and L. Genzel, Physica C **183**, 99 (1991).
- ²⁷D. E. Oates, A. C. Anderson, C. C. Chin, J. S. Derov, G. Dresselhaus, and M. S. Dresselhaus, Phys. Rev. B **43**, 7655 (1991).
- ²⁸H. F. Hess, R. B. Robinson, R. C. Dynes, J. M. Valles, Jr., and J. V. Waszczak, Phys. Rev. Lett. **62**, 214 (1989).
- ²⁹K. Karraï, E. J. Choi, F. Dunmore, S. H. Liu, H. D. Drew, Qi Li, D. B. Fenner, Y. D. Zhu, and Fu-Chun Zhang, Phys. Rev. Lett. **69**, 152 (1992).
- ³⁰Ch. Renner, A. D. Kent, Ph. Niedermann, Ø. Fischer, and F. Lévy, Phys. Rev. Lett. **67**, 1650 (1991).